THE ASTROPHYSICAL JOURNAL, 450:122–136, 1995 September 1

VLA OH OBSERVATIONS OF HIGH NEGATIVE VELOCITY GAS TOWARD SAGITTARIUS A WEST: A HIGH-VELOCITY CLOUD INTERACTING WITH THE GALACTIC CENTER

JUN-HUI ZHAO,[1] W. M. GOSS,[2] AND PAUL T. P. HO[1]
Received 1995 January 18; accepted 1995 March 14

ABSTRACT

The high negative velocity cloud in the direction of Sgr A* at -180 km s^{-1} was discussed by Güsten & Downes (1981) more than a decade ago. Since then, numerous observations have been carried out to determine the properties of this component; however, the nature of this feature was uncertain due to the lack of high angular resolution observations. Recently, we have carried out VLA observations of this feature in the H I and OH lines at $V_{LSR} = -180$ km s^{-1} with an angular resolution of several arcseconds. The OH 1667 MHz absorption is the best tracer of the gas in front of the continuum sources in the Galactic center. Both the structure and the kinematics have been determined, and we show that the high negative velocity absorbing gas is well mixed with the ionized gas in the center of the Galaxy. The mass of neutral gas seen in absorption at -180 km s^{-1} is about 5×10^3 $M_\odot$, only a small fraction of the entire cloud observed in CO emission. The observed kinematics are not consistent with ejection; outflow, or a possible association with the expanding molecular ring at $V = -135$ km s^{-1}. The location and morphology suggest that this high-velocity cloud may be tidally disrupted. Based on a numerical model, we demonstrate that the disrupted high-velocity gas can flow toward the Galactic center and interact with the central gravitational potential, thereby distorting the kinematics of the high-velocity gas projected in front of Sgr A West. This model also suggests that the minicavity 3″ southeast of Sgr A* could have resulted from the impact of a high negative velocity streamer. Both the morphology and the kinematics calculated in this model are consistent with the H92α observations of the central 10″ of the Galaxy as published by Roberts, Yusef-Zadeh, & Goss (1995).

Subject headings: Galaxy: center — ISM: clouds — ISM: kinematics and dynamics — radio lines: ISM

1. INTRODUCTION

Highly blueshifted absorption features toward the Galactic center were detected in the spectra obtained from early observations of H I (e.g., Sanders, Wrixon, & Mebold 1977). The absorbing gas at velocities between -210 to -160 km s^{-1} was confirmed by observations of both H_2CO and H I absorption lines (Güsten & Downes 1981). The origin of this high negative velocity gas (HNVG) was thought to be an ejection from the Galactic nucleus (Güsten & Downes 1981).

Some properties of the prominent kinematic features in the direction of Sgr A West (the spiral H II region; e.g., Ekers et al. 1983), which will be frequently referred to in this paper, are summarized: (1) The expanding molecular ring (EMR) is thought to be centered on the Galactic center with a radius of 200 pc (Scoville 1972). The typical velocity of the approaching EMR gas (which is located at the near side and is often observed in absorption) is -135 km s^{-1}, while the velocity of the receding gas (which is only observed in emission) is $+165$ km s^{-1}. (2) The most prominent kinematic features toward Sgr A West arise from the gas in the circumnuclear disk (CND) with a size of 2 pc × 3 pc, centered on Sgr A* (a compact radio source near the dynamic center). The rotating gas in the CND has radial velocities in the range from -100 to 100 km s^{-1} (e.g., Güsten et al. 1987; Roberts & Goss 1993) from the southwest to northeast. Finally, a distance of 8.5 kpc to the Galactic center is assumed throughout this paper; thus, the scale is $1'' \approx 0.04$ pc.

Recently, Marr et al. (1992) observed HCO^+ at 3 mm with an angular resolution of 8.″5 × 4″, imaging this absorption line at -180 km s^{-1} in the central 20″ of the Galactic center. HCO^+ was not detected at the position of Sgr A*, while it was detected at the surrounding positions. Pauls et al. (1993) then carried out VLA observations of H_2CO absorption at 6 cm in the D configuration with an angular resolution of 20.″6 × 9.″5. The authors did not detect the high negative velocity H_2CO gas at the position of Sgr A* and instead found it distributed northeast of the point source. Based on both the HCO^+ and H_2CO observations. Pauls et al. concluded that the HNVG must lie behind Sgr A*, falling into Sgr A West from behind.

Yusef-Zadeh, Lasenby, & Marshall (1993) presented an image of H I optical depth at $V = -185$ km s^{-1} observed using the VLA with an angular resolution of 25″. The elongated east-west morphology along the rotation axis of the CND leads the authors to conclude that the gas is expelled from the nucleus. They further suggested that the IRS 16 complex is the source driving this high-velocity gas.

In addition, Liszt & Burton (1993) imaged a 0.°45 × 0.°35 region about Sgr A* in CO emission with an angular resolution of ∼1′. They found that the negative-velocity gas at -190 km s^{-1} has an elongated shape with a larger extent (8 pc × 30 pc) than those obtained in the previous absorption observations of H I (5 pc × 15 pc), H_2CO (∼1 pc), and HCO^+ (∼1 pc). Based on these CO observations, the total H_2 mass is inferred to be $\sim 10^5$ $M_\odot$. The inferred kinetic energy is about

[1] Harvard-Smithsonian Center for Astrophysics, 60 Garden Street, MS 78, Cambridge, MA 02138.
[2] National Radio Astronomy Observatory, P.O. Box O, Socorro, NM 87801.

4×10^{52} ergs if the gas originates from the Galactic nucleus. Liszt & Burton argued that the -190 km s^{-1} gas may in fact be associated with the -135 km s^{-1} EMR (Scoville 1972) in front of the Galactic center at a distance of 200 pc from Sgr A*.

In this paper we present high angular resolution ($\sim 1''$) observations of H I at 21 cm and OH at 18 cm of the HNVG obtained with the VLA. At this resolution it is possible to determine whether the HNVG is in front of, or behind, or coincident with Sgr A*.

Furthermore, with the high-sensitivity OH observations, we are able to study the kinematics. In order to interpret the observed structures and kinematics, a numerical model was constructed. In this model, the HNVG presumably originates from a high-velocity cloud which is tidally disrupted within the central 100 pc and flows toward the nucleus from the far side of the Galactic center; the gas motion is governed by the central gravitational potential. We show that this model can reproduce the kinematics with a small fraction (about 5%) of the neutral gas, apparently having moved in front of the nucleus. We also discuss the kinematics of the H92α radio recombination line observed in the central 10′ of the Galaxy.

2. OBSERVATIONS

Table 1 summarizes the observational parameters for the VLA experiments carried out in 1991–1993. A spectral line mode with dual intermediate frequencies (IFs) at the 20 cm band was used. The 1991 observations was made during the Galactic center transient observations (Zhao et al. 1992) and have been discussed elsewhere. In all of our observations, we simultaneously observed H I and one of the OH Λ-doubling transitions. In order to study the high-velocity gas at -160 to -220 km s^{-1}, the observations were centered at the position of Sgr A*. The visibility data were calibrated using the radio sources NRAO 530 and 1748−253 for amplitude and phase calibration, and 3C 286 for bandpass calibration. The flux density scale was determined assuming the flux densities of 3C 286 are 14.86 and 13.75 Jy at 1420 and 1667 MHz, respectively.

The data were reduced using AIPS. Further phase corrections obtained from self-calibration of the continuum data were applied to all the line data. The continuum level was subtracted from the spectra in the visibility domain using the program UVLIN (Cornwell, Uson, & Haddad 1992). The typical rms noises are as listed in Table 1.

3. RESULTS

3.1. *Neutral Hydrogen Absorption*

The high-velocity H I absorption gas toward Sgr A* was detected at -210 km s^{-1} with S/N ≈ 3 in our 1991 observations with an angular resolution of $2'' \times 1''$ (see Zhao et al. 1992). The weak absorption line at this velocity is also marginally detected with S/N = 2.5 in both 1992 and 1993 observations with angular resolutions of $2'' \times 1''$ and $7'' \times 3''$, respectively. The H I opacity is 0.05 ± 0.015 with an angular resolution of $2'' \times 1''$.

3.2. *Hydroxyl Absorption*

In order to study the detailed structure of the HNVG, numerous spectra and images with angular resolutions in the range from 1″ to 7″ have been produced from the OH observations in the A and B configurations of the VLA.

3.2.1. OH *Absorption Spectra toward Sgr A**

Toward Sgr A*, we detect a prominent OH absorption feature at -180 km s^{-1} in both the 1667 and 1665 MHz transitions with an angular resolution of $2'' \times 1''$ (A-array data). These spectra are shown in Figure 1. The peak optical depths of the absorbing OH 1667 MHz and OH 1665, MHz lines are 0.07 ± 0.01 and 0.04 ± 0.01, respectively. The ratio τ(OH 1667 MHz)/τ(OH 1665 MHz) ≈ 1.8 agrees with that of an optically thin OH line in LTE. The FWHM velocity width is 18 km s^{-1} at a resolution of $2'' \times 1''$. Both the optical depth [τ(OH 1667 MHz) $\approx 0.11 \pm 0.01$] and the line width ($\Delta V_{\rm FWHM} \approx 31$ km s^{-1}) in the direction of Sgr A* increase significantly in spectra observed with a larger beam ($7'' \times 3''$) in the B configuration. This increase in opacity is due to a nonuniform distribution of the absorbing OH 1667 MHz gas in the vicinity of Sgr A*. The increase in line width indicates that a velocity gradient is present across Sgr A*. Note that, in contrast, neither the opacity nor the velocity width of the nearby

TABLE 1

H I/OH Observational Parameters

Parameter	Observing Date		
	1993 Apr 29	1992 Dec 30	1991 Jul 17
Rest frequency ν_0 (MHz) H I/OH	1420.406/1667.359	1420.406/1667.359	1420.406/1665.401
Channel separation $\Delta\nu$ (kHz)	97.7	97.7	97.7
Total channel number	127	127	127
Central channel	64	64	64
Hanning smoothing	Done off line	Done off line	Done off line
Central velocity $V_{\rm LSR}$ (km s^{-1})	−150	−150	0
Velocity coverage (km s^{-1})	650/550	650/550	650/550
Velocity resolution ΔV (km s^{-1})	10.3/8.8	10.3/8.8	10.3/8.8
Total observing time (hr)	1.5	4	2.5
Configuration	B	A	A
Field center (1950 epoch)	$\alpha = 17^h42^m29^s.32$	$\alpha = 17^h42^m29^s.32$	$\alpha = 17^h42^m29^s.96$
	$\delta = -28°59'18''.4$	$\delta = -28°59'18''.4$	$\delta = -28°59'34''.1$
Synthesized beam (HPBW)[a]	$8''.2 \times 3''.4/7''.0 \times 3''.0$	$2''.4 \times 1''.1/2''.0 \times 0''.9$	$2''.3 \times 1''.0/1''.9 \times 0''.9$
(P.A.)	(5°)/(5°)	(4°)/(4°)	(−9°)/(−9°)
Rms noise (mJy beam^{-1} channel^{-1})	9	5	7

[a] HPBW = half-power beamwidth.

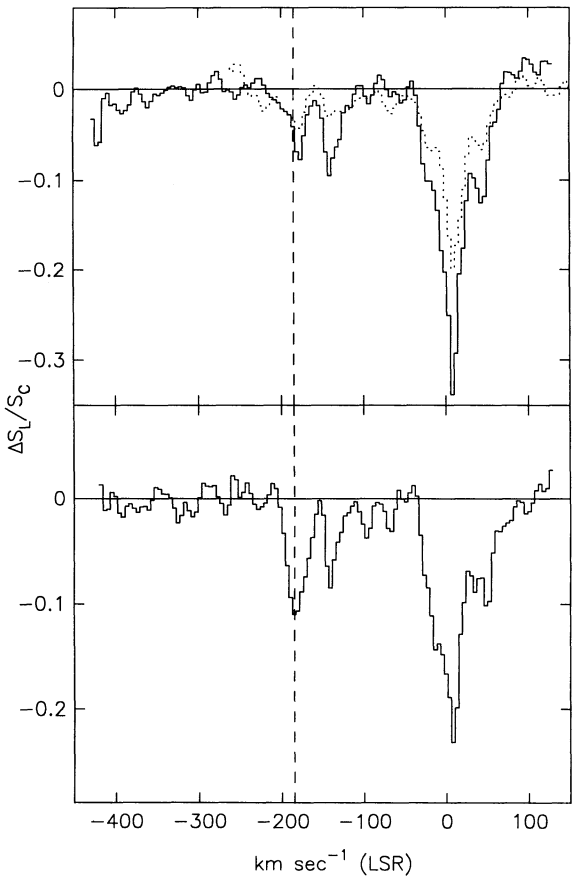

FIG. 1.—OH absorption components in the direction of Sgr A*. *Top*: OH 1667 MHz spectrum (*solid curve*) observed on 1992 December 30 in the A array with an angular resolution of 2".0 × 0".9 is compared with the OH 1665 MHz spectrum (*dotted curve*) observed 1991 July 17 with the same angular resolution. *Bottom*: OH 1667 MHz spectrum observed on 1993 April 29 in the B array with an angular resolution 7".0 × 3".0. The vertical dashed line is placed at −185 km s^{-1}.

spectral feature at −135 km s^{-1} changes with angular resolution. This suggests that the properties of −180 km s^{-1} gas are quite different from those of the −135 km s^{-1} gas. Note that because of the high contrast in continuum flux between Sgr A* and Sgr East, and the substantial absorption opacity in the OH lines, it is unlikely that the OH is behind Sgr A* and in front of Sgr A East.

Finally, since the OH 1667 MHz line transition appears to be stronger in absorption than the OH 1665 MHz, hereafter we will mainly discuss the HNVG based on the observations of OH 1667 MHz, and as a simplification, "OH" shall hereafter refer to OH 1667 MHz.

3.2.2. *Morphology of* OH *Absorption against Sgr A West and East*

In order to image the extended structure, it was necessary to use a lower angular resolution. The line and continuum images from the B array were convolved with a circular beam of 7". Figure 2 shows the resulting image of the OH absorption flux density integrated between −168 and −200 km s^{-1} (*solid contours*) in the central 4' of Sgr A West. The doubled-lined contour outlines Sgr A East (the possible supernova remnant [SNR] shell); the gray-scale representation shows the intensity of the continuum emission from both Sgr A West and East. The overall morphology of the OH absorption is elongated east-west with a size 3' × 1'. This elongation is consistent with the H I observations carried out by Yusef-Zadeh et al. (1993). The morphology of the OH gas in absorption is also characterized by a Z-shaped feature centered on Sgr A*. Note that the opacity of the absorbing gas at 7" resolution does not show the same morphology as the continuum source Sgr A East.

3.2.3. *Distribution of* OH *Optical Depth*

The visibility data observed in the A and B configurations during 1992 and 1993 were combined to improve the *uv* coverage. In order to determine both the fine structure of the OH opacity ($V_{LSR} = -180$ km s^{-1}) near Sgr A* and the kinematics of the extended OH line absorption, the images of opacity for individual channels were convolved with a circular beam of 5". The rms noises are 5 and 6 mJy beam^{-1} for the line channel and continuum images, respectively. The optical depths were determined using cutoffs of 3.5 σ (1 σ = rms) in the line images and 6 σ in the continuum images. Figure 3 shows the channel images of the optical depth of this component. The relative errors in optical depths are typically 20% or less. Figure 4 shows the optical depth (*top*) at −185 km s^{-1} and the relative errors of the optical depth (*bottom*). This derivation of the optical depth and the errors provide the true optical depth of the molecular cloud only if the cloud is located in front of the continuum sources. In the case in which the cloud is located inside or behind the continuum sources, the derived optical depth underestimates the true optical depth of the feature.

Figure 5 shows an image of the integrated optical depth in the velocity range −157 to −230 km s^{-1} at 5" angular resolution. The distribution of the OH optical depth appears to be nonuniform over Sgr A West. In particular, a noticeable region with lower optical depth or an OH cavity) is centered northeast of but including Sgr A*. The decreased optical depth in the region within 7" of Sgr A* is consistent with the previous observations of HCO^+ and H_2CO (Marr et al. 1992; Pauls et al. 1993). The OH observations do show a significant optical depth within this OH cavity. At the cavity center, the peak optical depth is τ(OH 1667 MHz) = 0.04 ± 0.01 (at $v = -170$ km s^{-1}). At the position of Sgr A*, τ(OH 1667 MHz) ≈ 0.08 ± 0.005 (at $v = -182$ km s^{-1}) with a resolution of 5".

Another OH optical depth cavity at −180 km s^{-1} is observed in the region northwest of the Galactic center transient 36" southeast of Sgr A* (Zhao et al. 1992). The minimum opacity in this region is τ(OH 1667 MHz) < 0.04. There is a dense molecular cloud at $V_{LSR} = +20$ km s^{-1} observed in both NH_3 (Ho et al. 1991) and OH (Zhao et al. 1992) toward this region.

In addition, a few obvious filaments of OH are observed. Filament N is located 25" north of Sgr A*, extended in an east-west direction with a length of 2'. This OH filament corresponds to the radio continuum filament across the northern arm of Sgr A West (e.g., Ekers et al. 1983). Filament S is located southeast of Sgr A West with an L-shaped morphology. The integrated OH optical depth is typically $\int \tau$(OH 1667 MHz) dv = 5–8 km s^{-1} in these filaments.

Finally, Figure 5 shows a clump of large optical depth in the region 25" southwest of Sgr A*. The integrated optical depth [$\int \tau$(OH 1667 MHz) dv] is greater than 8 km s^{-1}. The channel images (Fig. 4) reveal that the peak in optical depth of the OH

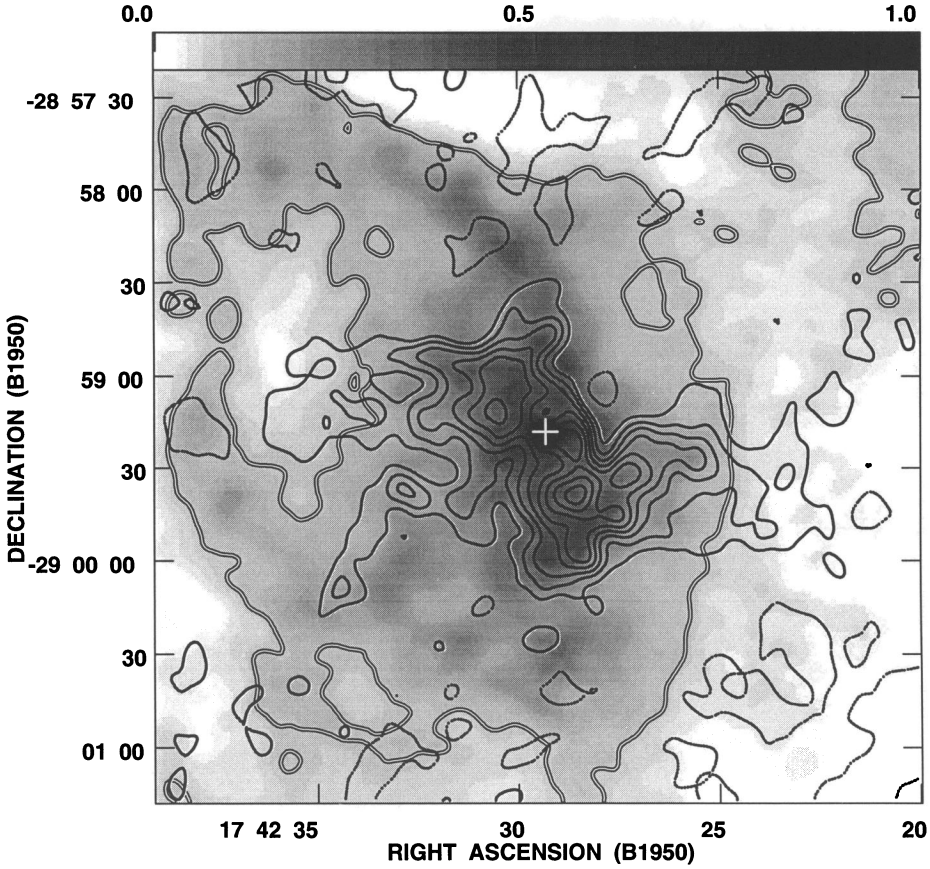

FIG. 2.—Bold contours represent the OH 1667 MHz absorption image of the HNVG gas averaged within a velocity range between -168 and -200 km s^{-1} observed using the VLA in the B configuration with an angular resolution of 7″. The contour levels are -21, 14, 28, 42, 56, 70, 84, 98, and 112 mJy beam^{-1}. The gray-scaled representation (0–1 Jy beam^{-1}) is the radio continuum emission at 18 cm obtained from the line-free channels. The double-lined contour at 0.1 Jy beam^{-1} indicates the emission from the Sgr A East shell. The cross indicates the position of Sgr A*.

clump is located southwest of Sgr A* at $\Delta\alpha = -30''$ and $\Delta\delta = -10''$. At this position, the peak optical depth of OH 1667 MHz is saturated [τ(OH 1667 MHz) > 1.5] at -168 km s^{-1} with a FWHM line width of ~ 9 km s^{-1}.

3.2.4. *Distribution of Radial Velocity and Velocity Dispersion*

The distributions of both the optical-depth–weighted radial velocity ($\bar{V}$) and velocity dispersion (σ_v) are shown in Figures 6 and 7. A large change in velocity of 60 km s^{-1} in the direction north to south is observed. A similar velocity gradient was also noticed in the H I observations by Yusef-Zadeh et al. (1993). The velocity gradient appears to be consistent with the sense of rotation of the CND on a similar angular scale ($\sim 2'$), but the magnitude of the gradient is smaller by at least a factor of 6. In addition, the typical values of the velocity dispersion are in the range 5–10 km s^{-1}, but increase to 15–20 km s^{-1} in the vicinity of the clump southwest of Sgr A* ($\Delta\theta = 15''$–$20''$).

Figure 8 shows a group of velocity-declination images at various right ascensions within the central 200″ × 100″ region of Sgr A*. In the images displaced 30″ and 40″ to the east, the absorption feature of filament N is prominent. The images displaced 20″ and 10″ to the east show an extended structure near -180 km s^{-1} with an obvious velocity gradient of 30 km s^{-1} arcmin^{-1}. Note that the -135 km s^{-1} EMR feature shows no significant gradient. In the image that includes Sgr A*, a highly disturbed feature is seen 15″ south of Sgr A*, with a velocity wing that extends to -235 km s^{-1}. This feature becomes prominent 10″ to the west and continues to be observed to the west before fading at a distance of 1′.

In addition, there is an extended diffuse feature near -100 km s^{-1}, south of Sgr A*. This feature is consistent with the kinematics of the rotating gas in the CND.

3.2.5. *Comparison between* OH *Opacity and Radio Continuum*

A higher angular resolution is necessary for making a comparison between the distributions of OH opacity ($V = -180$ km s^{-1}) and the radio continuum features without contamination by the diffuse emission in Sgr A West. The high resolution also separates the OH cavity to the northeast from Sgr A*. On the other hand, the short baselines are needed to increase the S/N for imaging the extended OH absorption features toward Sgr A West. Using the data from the A and B arrays with uniform weighting, an angular resolution of 3″ × 3″ is achieved. In Figure 9, a continuum image (*white solid contours*) of Sgr A West is superposed on the gray-scale image of the optical depth of the HNVG averaged over the seven channels between -168 and -194 km s^{-1} The solid black contour outlines the optical depth of 0.1. At this resolution, the cavity in OH opacity is well resolved with a size of 20″ (0.8 pc). The well-known continuum features in Sgr A West such as Sgr A*, the northern and eastern arms, and the western arc can be separated from the diffuse continuum emission (Ekers et al.

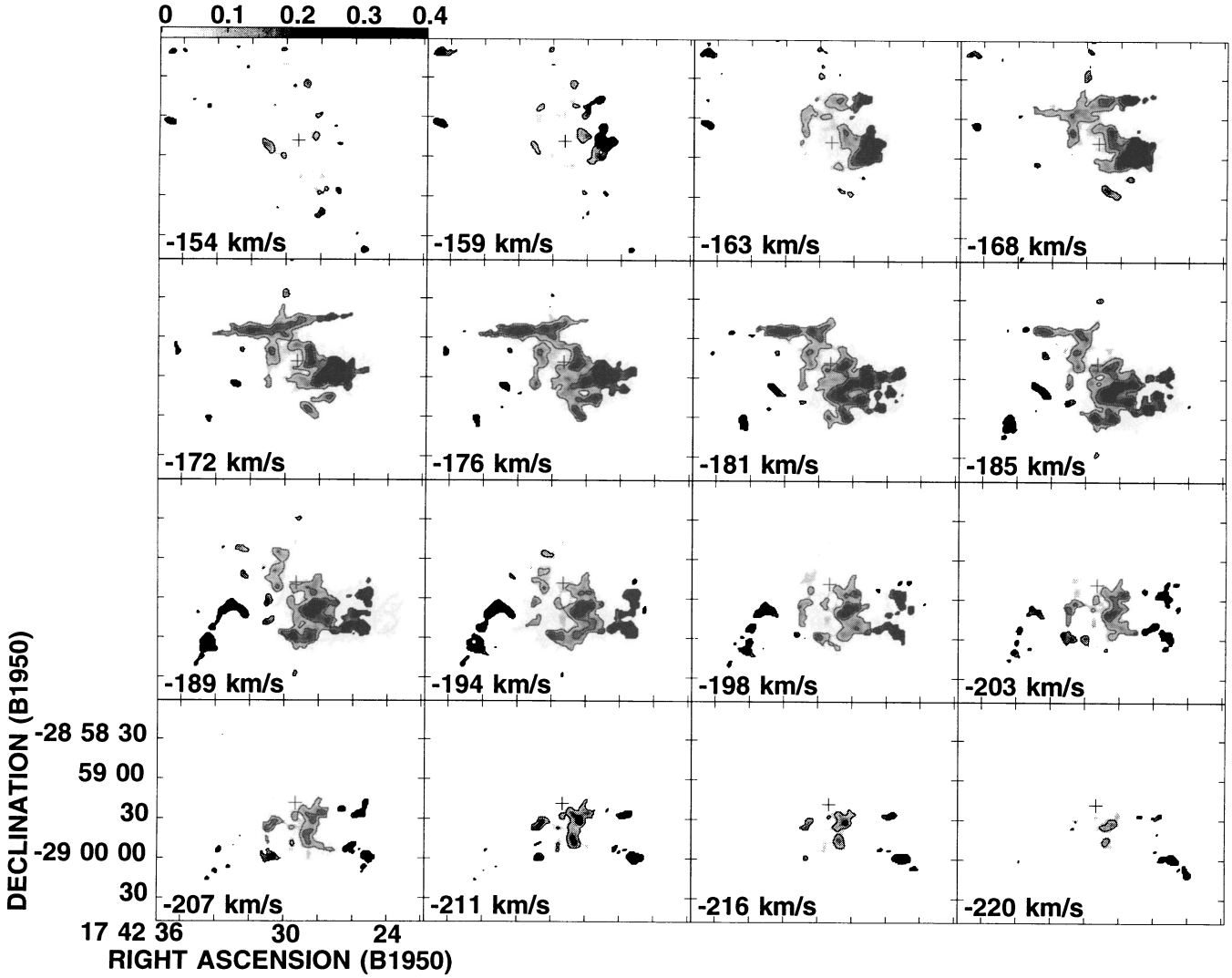

FIG. 3.—Channel images of the optical depths of OH 1667 MHz in a velocity range between −154 and −220 km s^{-1}. The contour levels indicate τ(OH 1667 MHz) = 0.1, 0.2, 0.3, and 0.4. The gray scale represents the opacity on a linear scale from τ(OH 1667 MHz) = 0 to 0.4. The cross indicates the position of Sgr A*. The resolution is 5″.

1983). The clumps of optical depth distribution are clearly seen against the various continuum features. Sgr A* is located at the southwestern rim of the OH cavity, about 6″ from the center of the cavity. At the position of the continuum emission from the northern and eastern arms, the OH opacity is quite low [$\bar{\tau}$(OH 1667 MHz) = 0.05 ± 0.01] while the filaments N and S and the western arc correspond to larger OH opacity [τ(OH 1667 MHz) > 0.15].

4. INTERPRETATION

4.1. *Location and Morphology*

The presence of an absorption line at $V = -180$ km s^{-1} in the direction of Sgr A* (see Fig. 1) is direct evidence that at least part of the HNVG is located between Earth and the Galactic nucleus. This conclusion is contrary to the result suggested by Pauls et al. (1993), who place Sgr A* in front of the HNVG. There are no indications that the HNVG is associated with Sgr A East (a possible SNR) located beyond Sgr A West (Pedlar et al. 1989). The larger optical depth against the radio continuum filament across the northern arm of Sgr A West suggests that the continuum filament is likely located at the far side of the Galactic center and the HNVG may extend beyond Sgr A West. Neither the EMR model by Liszt & Burton (1993) nor the outflow/ejection model by Güsten & Downes (1981) and Yusef Zadeh et al. (1993) could explain the HNVG if it were located beyond the Galactic center. Moreover, that the morphology of the HNVG is well centered on Sgr A* provides evidence that the HNVG is physically associated with the Galactic center (Figs. 2 and 5). The overall east-west elongation may result from interactions between the HNVG and the Galactic center.

4.2. *Relationship between* OH *Cavity, Warm Dust, and* He I *Line Stars*

Figure 10*a* shows the comparison between the OH opacity distribution and the infrared emission at 12.4 μm in the vicinity of the OH cavity. The 12.4 μm was observed by Gezari (1992) with an angular resolution of 1″. A good correlation between the dust and ionized gas in the central region was previously found by Gezari & Yusef-Zadeh (1990). These authors concluded that the warm dust grains and the ionized gas are well

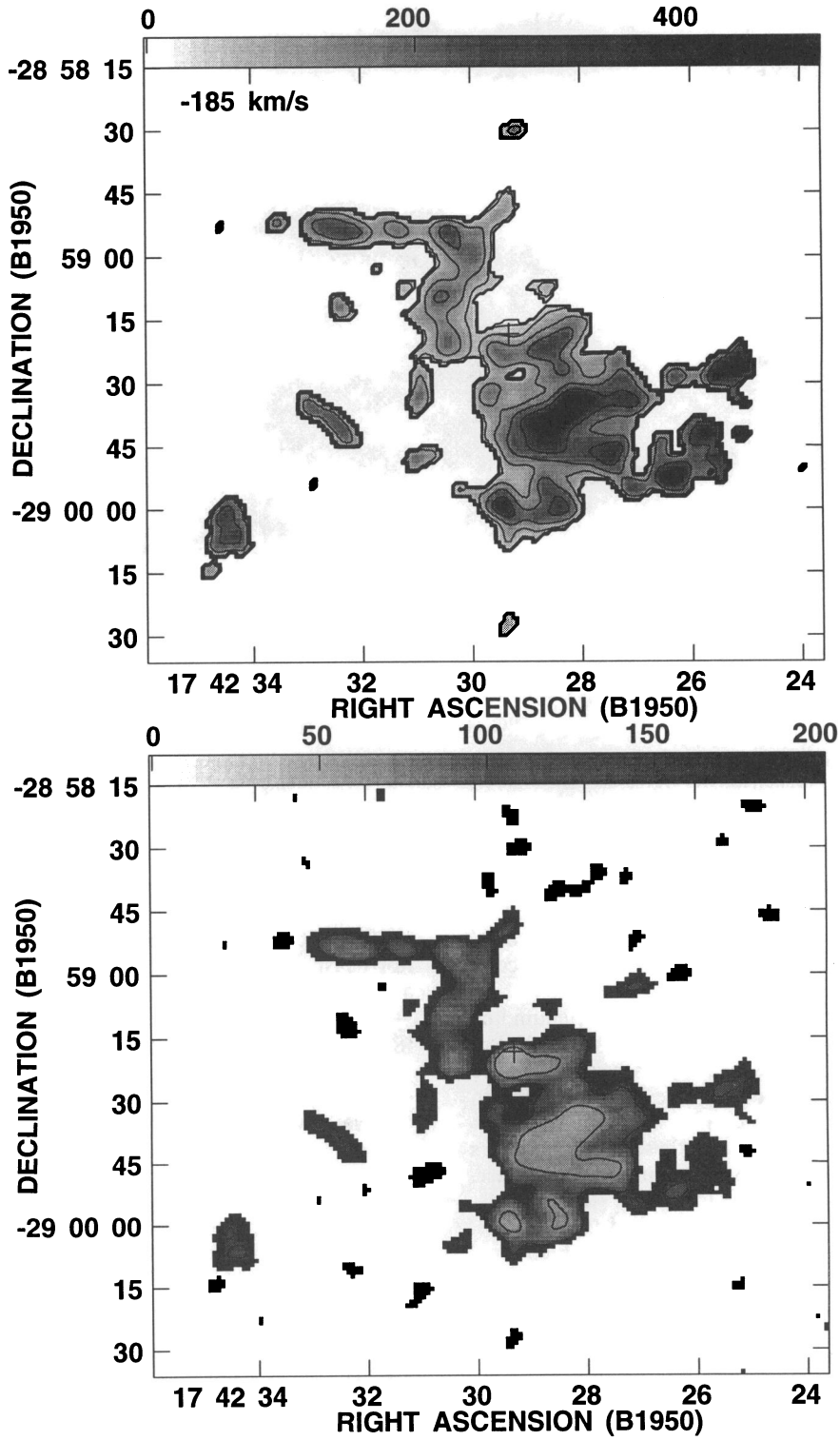

FIG. 4.—*Top*: Optical depth, τ(OH 1667 MHz), at a velocity of -185 km s^{-1}. The gray-scale representation indicates a range of optical depth from 0 to 0.5. The contour levels indicate τ(OH 1667 MHz) = 0.02, 0.04, 0.08, 0.14, 0.22, and 0.32. *Bottom*: Relative errors of optical depth ($\Delta\tau/\tau$) correspond to the optical depth image. The gray-scale representation indicates a range of errors between 0% and 20% of the optical depths. Contour levels are 4%, 8%, and 16% of the optical depths. The cross indicates the position of Sgr A*.

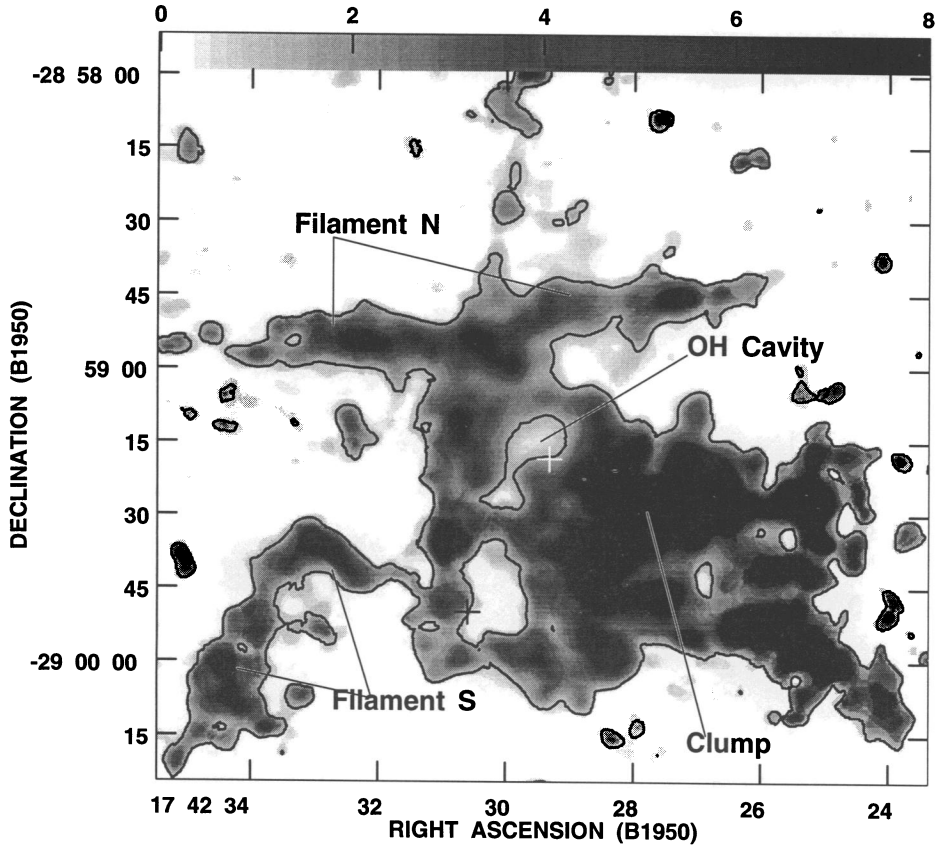

FIG. 5.—Image of optical depth integrated over a velocity range between -157 and -230 km s^{-1}. The contour is an integrated optical depth [$\int \tau$(OH 1667 MHz)dv] of 1.5 km s^{-1}. Several absorption features are marked. The white cross indicates the position of Sgr A*. The cross 36″ southeast of Sgr A* is the position of the Galactic center transient.

mixed in the central parsec of the Galaxy. From Figure 10, we find that the mid-infrared emission feature fits inside the OH ($V_{LSR} = -180$ km s^{-1}) cavity to the northeast. The correlation is evidence that the energy source for both the radio continuum and mid-infrared emission could result in the presence of the OH cavity at $V_{LSR} = -180$ km s^{-1}.

Krabbe et al. (1991) detected a cluster of compact helium line sources with broad line widths from $\sim$100 to over 1000 km s^{-1} distributed in the central parsec. The observations of the He I line stars provide evidence for massive star formation in the past 10^6 yr in the central parsec of the Galaxy. The overabundance of helium determined from these He I line stars suggests that the stars are in their post–main-sequence phase. The mass-loss rate is estimated to be from 10^{-5} to 10^{-4} $M_\odot$ yr^{-1}, and the outflow velocity is between 500 and 1000 km s^{-1}. A total luminosity of 1.2×10^7 $L_\odot$ from the cluster of He I line stars can account for nearly the entire infrared luminosity of the central few parsecs. The He I line stars are likely to be the major heating sources for the warm dust (Gezari 1992) and may significantly contribute to the ionization of Sgr A West (Krabbe et al. 1991).

We have superimposed the positions of the H I line sources on the OH optical depth image (Fig. 10*b*). The majority of the He I sources appear to be located near Sgr A* or near IRS 16 but not at the OH cavity center. The spatial correlation between the distributions of OH optical depth, warm dust, and positions of the He I line sources suggests that the hot He I stars could be the sources of heating and ionization in the central region. The OH cavity suggests that the molecular gas at -180 km s^{-1}, exposed to the strong UV radiation field in the vicinity of the He I line stars, can be ionized and/or dissociated. In fact, a diffuse ionized component at $V_{LSR} = -130$ to -195 has been detected (Yusef-Zadeh, Zhao, & Goss 1995) 10″ northeast of Sgr A*, where the OH cavity ($V_{LSR} = -180$ km s^{-1}) is located and a compact ionized component at -100 to -300 km s^{-1} has also been observed 5″ southwest of Sgr A* (Roberts & Goss 1993; Roberts, Yusef-Zadeh, & Goss 1995). The unique kinematics and location suggest that the ionized components are likely parts of the HNVG that are physically associated with the Galactic center.

4.3. *Physical Properties*

The average optical depth at -185 km s^{-1} over the entire OH 1667 MHz absorption region (1′ × 3′) is $\sim$0.15 with a typical FWHM line width of 25 km s^{-1}. The OH column density $\langle N$(OH 1667 MHz)$\rangle$ of the molecular cloud is estimated to be 9×10^{15} cm^{-2}. Assuming the fractional abundance of OH 1667 MHz to H_2 is 6×10^{-7} (Herbst & Leung 1989), the H_2 column density is 1.5×10^{22} cm^{-2}. The inferred total H_2 mass of this cloud is then 5×10^3 $M_\odot$, consistent with the estimates inferred from H I and H_2CO absorption observations (e.g., Güsten & Downes 1981; Yusef-Zadeh et al. 1993). This total mass is, however, much less than the mass of 10^5 $M_\odot$ derived from the CO emission observations with an extent of 30 pc. If the chemical abundances are correct, the absorbing cloud in front of the numerous continuum sources in the Galactic center would appear to be a small fraction (5%) of the entire -185 km s^{-1} cloud observed in CO emission.

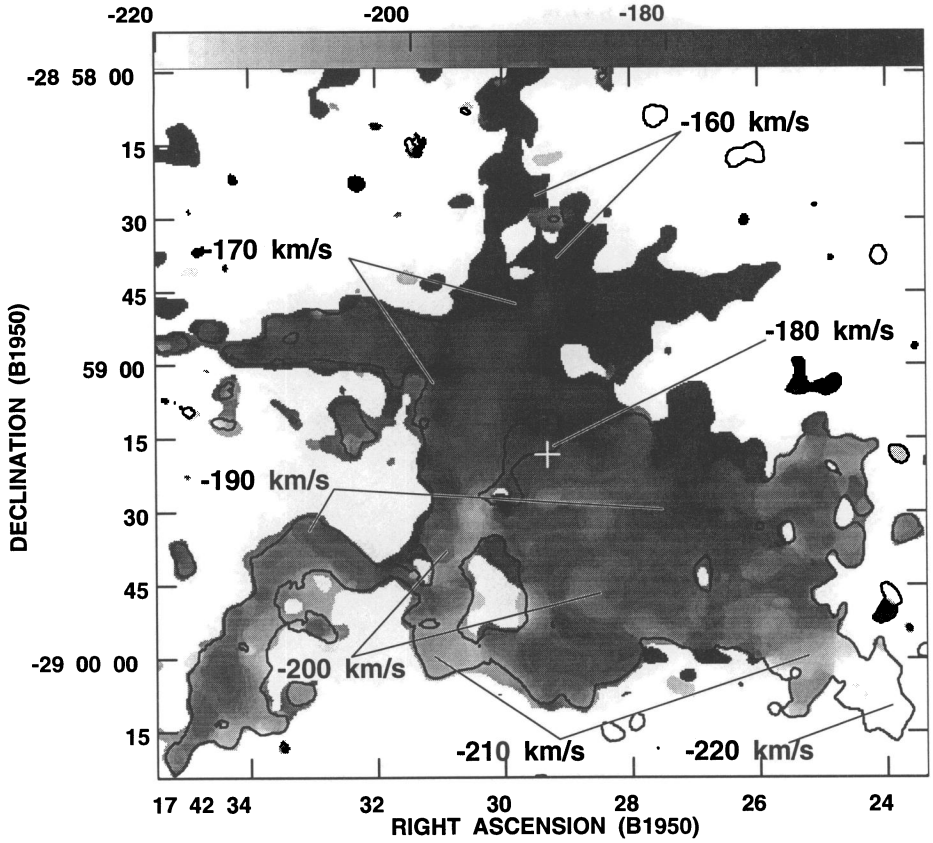

FIG. 6.—Image of the velocity distribution weighted by the optical depth. The angular resolution is 5″. The contour indicates an integrated optical depth [$\int \tau$(OH 1667 MHz)dv] of 1.5 km s^{-1}.

Table 2 summarizes the properties of the HNVG gas obtained from the OH 1667 MHz absorption and CO emission observations.

4.4. *Kinematics*

4.4.1. *Gas in the EMR and the CND*

The HNVG component of the OH gas is centered at -180 km s^{-1}, which is well separated from the gas in the near part of the EMR (-135 km s^{-1}). There is no significant velocity gradient observed for the -135 km s^{-1} component, with a nearly constant velocity across the central 3 pc region. This result is consistent with the proposal that the EMR has a much larger radius (200 pc) (Scoville 1972). While the EMR shows large-scale curvature in a position-velocity diagram, the typical velocity gradient near Sgr A* is less than 1 km s^{-1} arcmin^{-1} (Liszt et al. 1977). Both the velocity gradient (30 km s^{-1} arcmin^{-1}) and the larger velocity dispersion ($\sigma_V \sim 20$ km s^{-1}) of the OH gas close to Sgr A* suggest that the HNVG gas is closer to the Galactic center than the EMR gas.

TABLE 2

PHYSICAL PROPERTIES OF THE HNVC

Parameters	OH 1667 MHz Absorption	CO(1–0) Emission
Mean optical depth	$\langle\tau\rangle = 0.15$	...
Line width	$\Delta V_{\rm FWHM} = 25$ km s^{-1}	...
Angular size	$3' \times 1'$	$0.^{\circ}2 \times 0.^{\circ}05$
Linear size	7.4×2.5 pc^2	30×7.4 pc^2
OH column density ($N_{\rm OH}$)	8.7×10^{15} cm^{-2}	...
H_2 column density (N_{H_2})	1.4×10^{22} cm^{-2}	6×10^{21} cm^{-2}
Total H_2 mass (M_{H_2})	$4.2 \times 10^3\ M_\odot$	$10^5\ M_\odot$

The rotating gas in the CND is believed to show circular orbital motion with a radius of 1.5 pc, a rotation velocity of 105–110 km s^{-1}, and an inclination angle of 60° (e.g., Schwarz, Bregman, & van Gorkom 1989; Roberts & Goss 1993; Güsten et al. 1987; Jackson et al. 1993). The kinetic energy of the HNVG gas is at least 3 times larger than that of the circularly rotating gas of the CND and greatly exceeds the potential energy. Thus, the motion of the HNVG gas is distinctly different compared to the circular orbital motion of the gas in the CND.

4.4.2. *Bipolar Outflows or Ejection from the Nucleus*

Both outflow and ejection phenomena have been observed in extragalactic nuclei. There have been previous suggestions that the HNVG could arise from an ejection by the Galactic nucleus (Güsten & Downes 1981). The driving force is thought to be the radiation pressure both from recent bursts of star formation and from an accretion disk around a massive black hole. Based on recent lower resolution VLA H I observations, Yusef-Zadeh et al. (1993) further suggest that the HNVG gas is an outflow accelerated by the energy sources of the IRS 16 cluster along with the He I emission stars.

If the HNVG had originated from the Galactic center, the age of the KNVG cloud would be at most 1.5×10^5 yr. This timescale is an order of magnitude less than the typical ages of the giant stars in the central parsec (Allen, Hyland, & Hillier 1990; Krabbe et al. 1991). The mass-loss rate integrated over

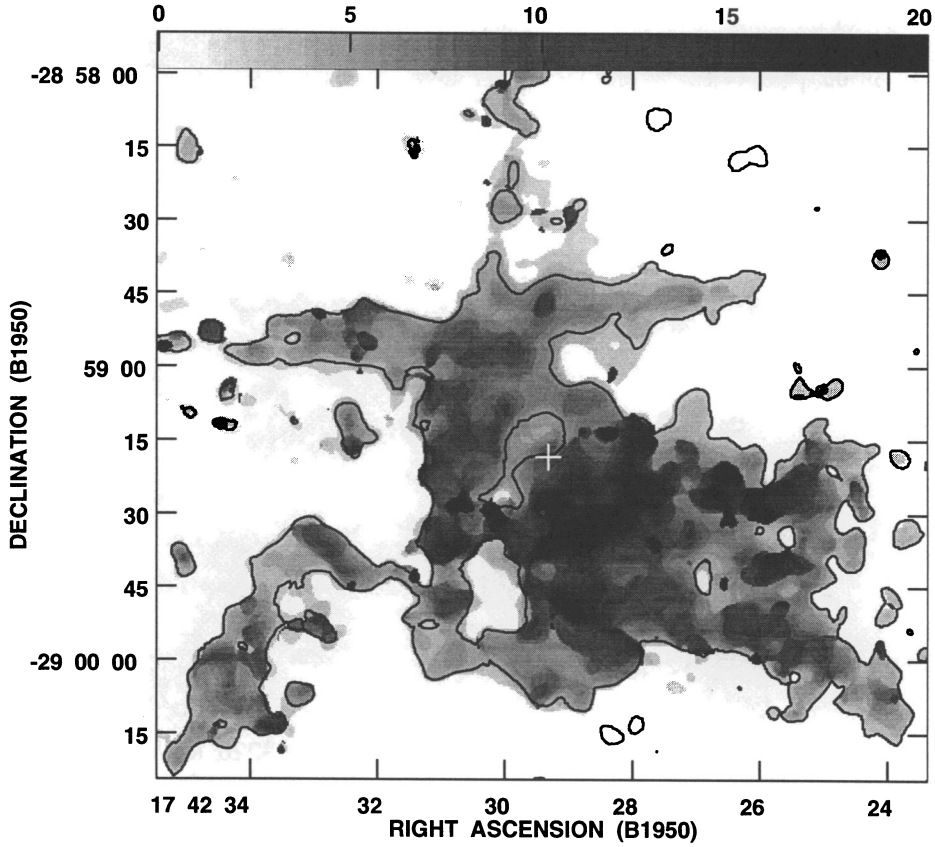

FIG. 7.—Image of the velocity dispersion weighted by the optical depth with an angular resolution of 5″. The contour indicates an integrated optical depth [$\int \tau$(OH 1667 MHz)dv] of 1.5 km s^{-1}.

the possible energy sources including the IRS 16 cluster and the He I emission stars is about $5 \times 10^{-3}\ M_\odot\ \mathrm{yr}^{-1}$. For a mean velocity of 700 km s^{-1}, the total mechanical power is 8×10^{38} ergs s^{-1}, or 3×10^{46} ergs yr^{-1}. This energy output seems to be insufficient to account for the total kinetic energy of 4×10^{52} ergs in the entire HNVG cloud as estimated from the CO observations (Liszt & Burton 1993), although a more complex acceleration mechanism (e.g., Yusef-Zadeh et al. 1993) might be applicable. In addition, the ejection or outflow models are difficult to explain due to the absence of highly redshifted gas at a velocity of approximately +200 km s^{-1} which would correspond to the motion of the gas on the far side of the Galactic center.

5. A NEW MODEL

It is necessary to summarize all relevant observations before proposing a new model. The OH 1667 MHz absorption is the best tracer of the gas in front of the continuum sources. The distorted kinematics of the absorbing OH 1667 MHz gas at −180 km s^{-1} along with the fact that an ionized component with higher negative velocities (−200 to −300 km s^{-1}) is located close to Sgr A* (Roberts et al. 1995) suggest that the HNVG may be physically associated with the Galactic center. In addition, properties of the large-scale CO emission gas at −180 km s^{-1} within the central several arcminutes have been further investigated using the James Clerk Maxwell Telescope with an angular resolution of 20″ in several CO transitions (Marshall & Lasenby 1994, 1995). The new CO observations show that the majority of the HNVG gas traced by the CO (2–1) is cold, without significant velocity gradient, and similar to the gas in the large-scale distribution observed in CO (1–0) by Liszt & Burton (1993). A stronger emission component traced by CO (3–2) is also observed at −200 to −300 km s^{-1} within 1′ (2 pc) southwest of Sgr A* with a large linewidth (50 km s^{-1} (Marshall & Lasenby 1995). This shows that the CO gas close to Sgr A* is indeed heated and accelerated by the Galactic center. All the existing observations appear to be consistent with the idea that the HNVG is impacting on the Galactic center and interacting with the central gravitational potential. The Galactocentric radius of the tidally unstable zone for a cloud with a typical mass of $10^5\ M_\odot$ and a size of 10 pc is believed to be as large as 100 pc (Güsten & Downes 1980). Thus, the central gravitational potential could essentially disrupt such a cloud within this tidal zone and pull the gas into the central potential well. In the CO images obtained by Liszt & Burton (1993), an elongated east-west ridge at −187 km s^{-1} which connects a CO clump to the Galactic center may be interpreted as a result of tidal disruption. The projected length of the CO emission feature. We, therefore, propose that the HNVG observed in absorption toward Sgr A West is part of the disrupted cloud and has moved to the nucleus under the direct influence of the central gravitational potential. The HNVG gas near Sgr A* is not only accelerated by the central gravitation force but also heated or ionized by the central energy sources.

5.1. *Kinematic Evidence for a Cloud Interacting with the Central Gravity*

In this section we provide a numerical model to calculate the kinematic characteristics of a high-speed molecular flow which

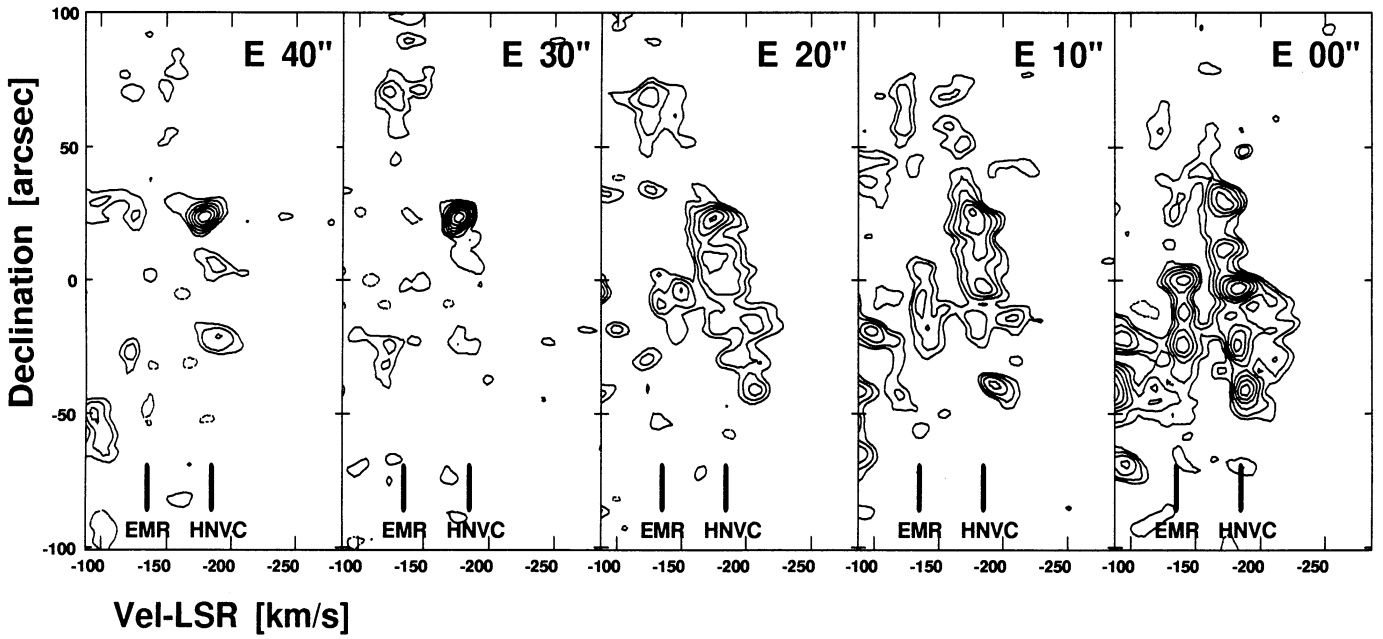

FIG 8*a*

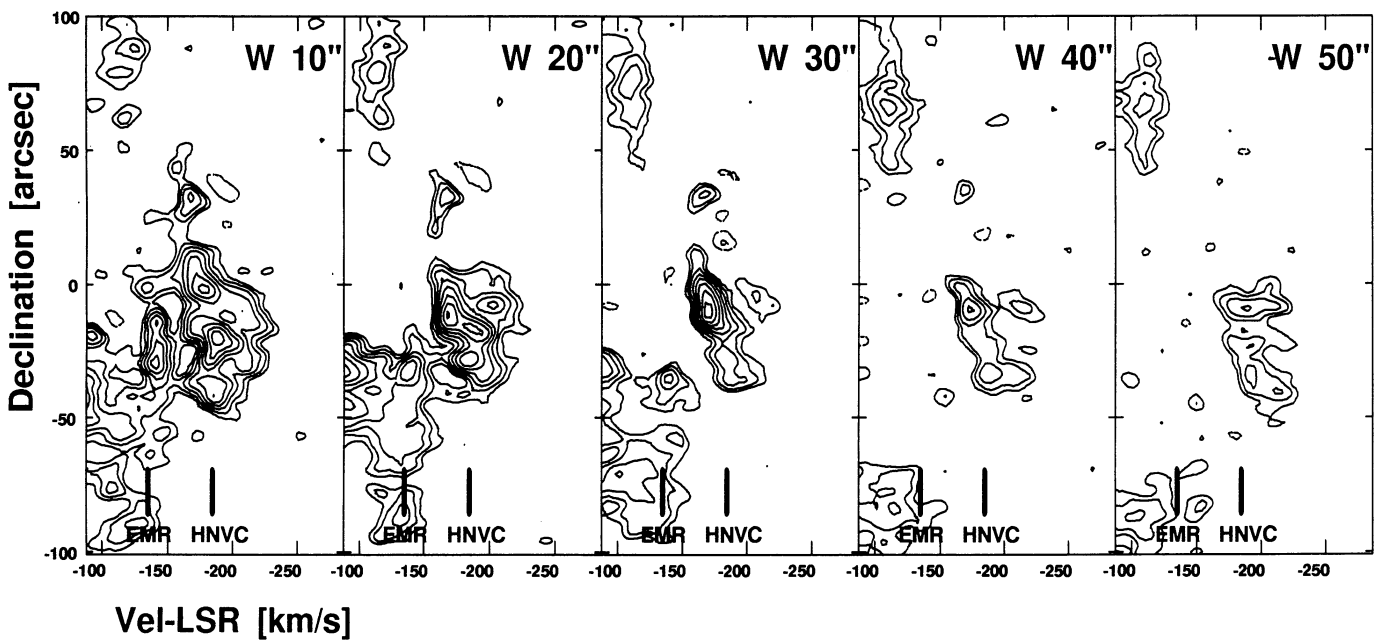

FIG. 8*b*

FIG. 8.—(*a*) Velocity-declination distribution of the OH 1667 MHz absorption produced by averaging a strip of 10″ in right ascension. The vertical axis indicates declination offsets from the position of Sgr A*. The horizontal axis indicates the LSR radial velocity. (*b*) Continuation of (*a*).

strongly interacts with a central massive gravitational force. As a simplifying assumption, we treat the molecular gas elements in the flow as particles and assume that the gas elements only interact with the central potential well. The trajectory of each incident particle will be a hyperbola. As a particle approaches the center, it will be attracted and its orbit will deviate from the incident straight-line trajectory. The final direction of motion is therefore not the same as the incident direction, and the deviation angle (ϕ, the angle between the incident and final directions) can be calculated by the following:

$$\phi = 2 \arctan\left(\frac{GM}{V_0^2 b}\right),$$

where V_0 is the incident velocity and b is the impact parameter defined as the perpendicular distance between the center of the gravitation field and the incident velocity vector, M is the mass of the central gravitational source, and G is the gravitational constant.

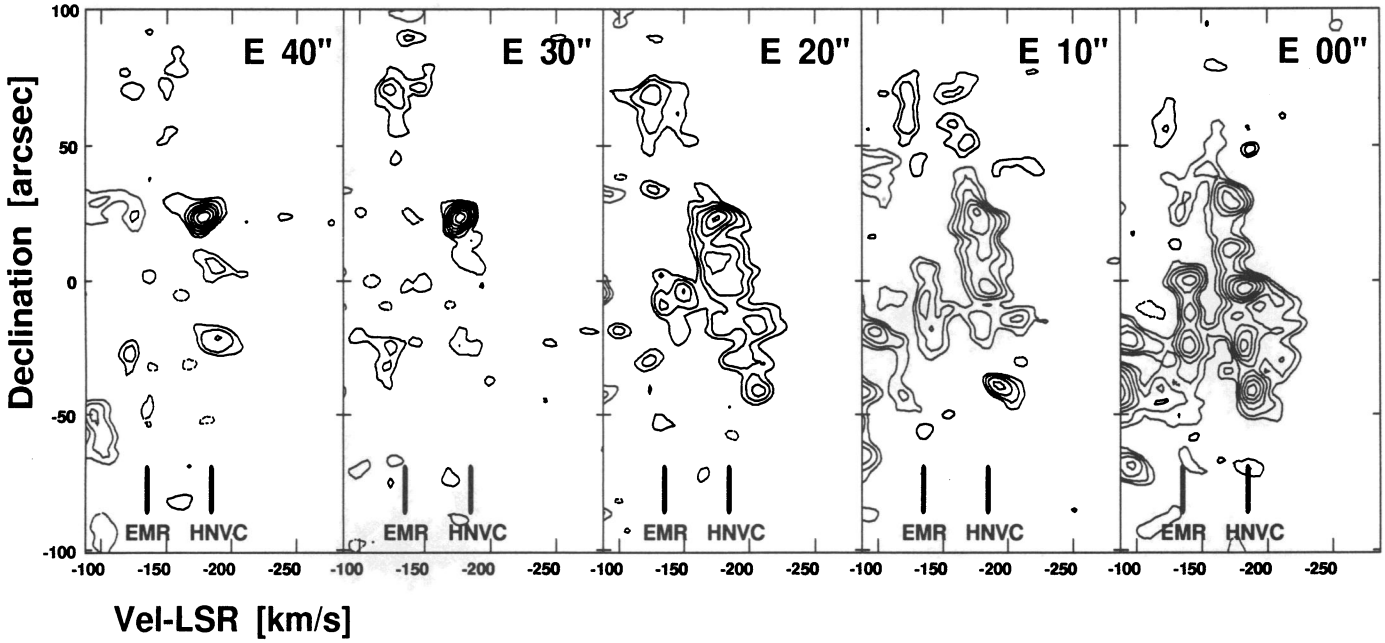

FIG 8*a*

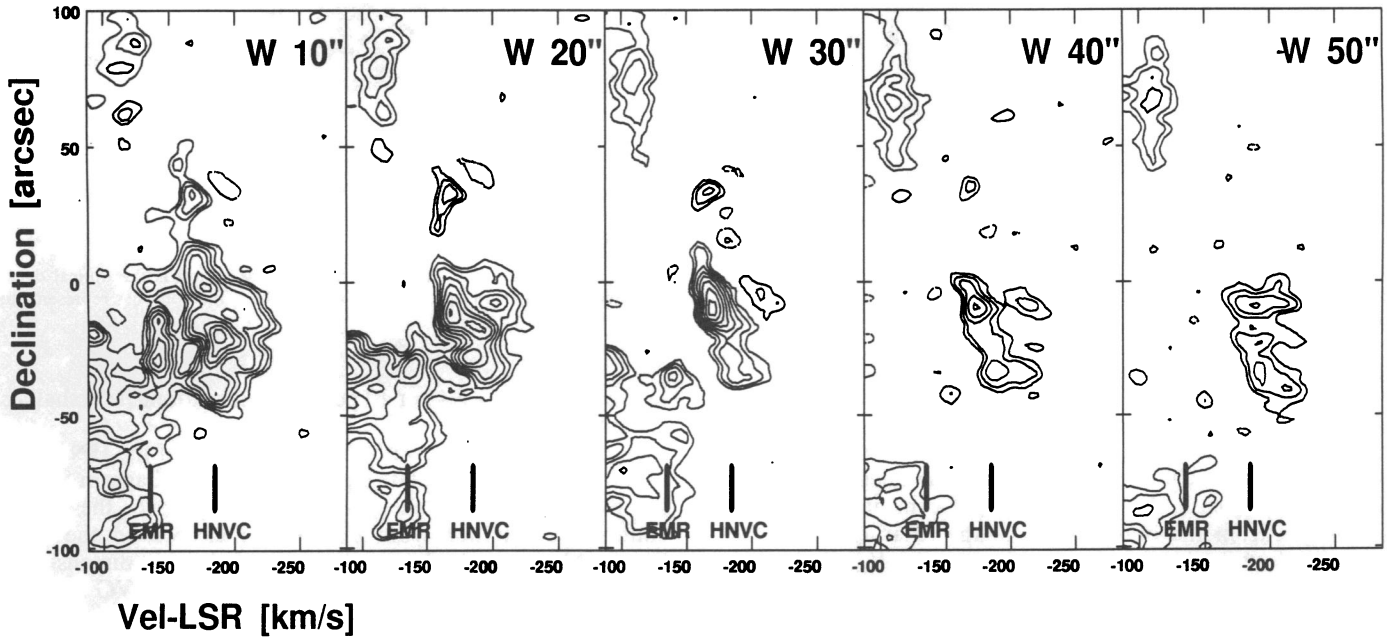

FIG 8*b*

FIG. 8.—(*a*) Velocity-declination distribution of the OH 1667 MHz absorption produced by averaging a strip of 10″ in right ascension. The vertical axis indicates declination offsets from the position of Sgr A*. The horizontal axis indicates the LSR radial velocity. (*b*) Continuation of (*a*).

strongly interacts with a central massive gravitational force. As a simplifying assumption, we treat the molecular gas elements in the flow as particles and assume that the gas elements only interact with the central potential well. The trajectory of each incident particle will be a hyperbola. As a particle approaches the center, it will be attracted and its orbit will deviate from the incident straight-line trajectory. The final direction of motion is therefore not the same as the incident direction, and the deviation angle (ϕ, the angle between the incident and final directions) can be calculated by the following:

$$\phi = 2 \arctan\left(\frac{GM}{V_0^2 b}\right),$$

where V_0 is the incident velocity and b is the impact parameter defined as the perpendicular distance between the center of the gravitation field and the incident velocity vector, M is the mass of the central gravitational source, and G is the gravitational constant.

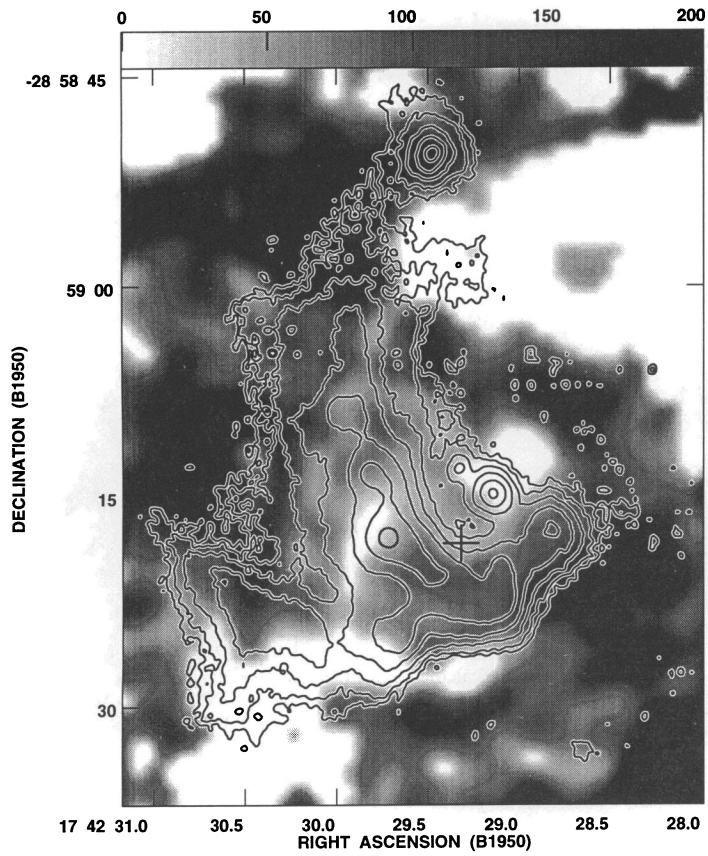

FIG. 10*a*

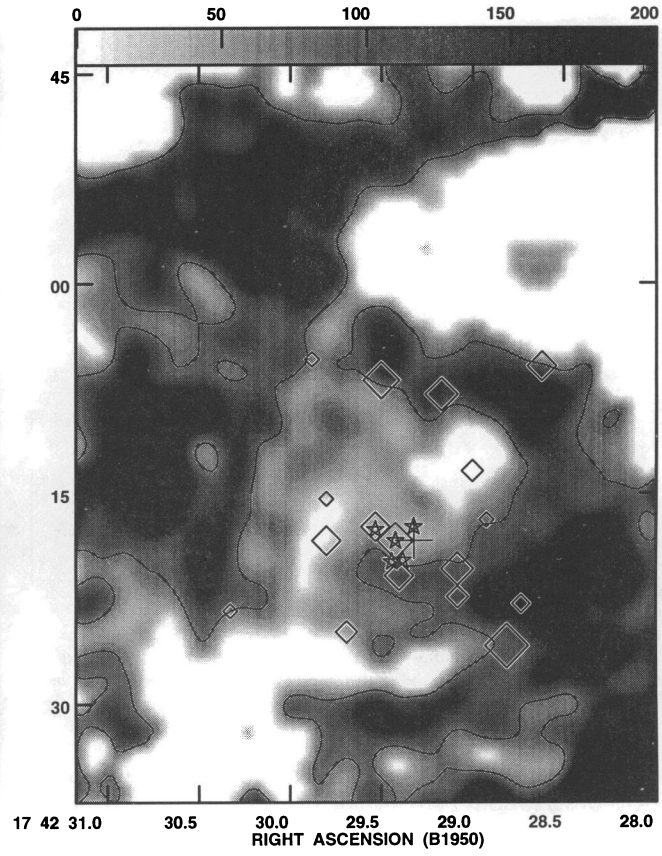

FIG. 10*b*

Fig. 10.—(*a*) Comparison between OH 1667 MHz optical depth and the mid-infrared emission; the gray-scale representation indicates the optical depth of OH 1667 MHz absorption averaged in a velocity range between -165 and -195 km s^{-1}. The contours represent the 12.4 μm emission observed by Gezari (1992). (*b*) Comparison between OH 1667 MHz optical depth and He I line sources. The gray-scale representation indicates the OH 1667 MHz optical depth from $\langle\tau(\text{OH 1667 MHz})\rangle \leq 0.01$ (*white*) to $\langle\tau(\text{OH 1667 MHz})\rangle = 0.2$ (*black*). The contour outlines the level of $\langle\tau(\text{OH 1667 MHz})\rangle = 0.1$. The size of the diamond is proportional to the flux of the He I line. The stars indicate the IRS 16 complex.

possible range for the incident angle is $10° < \alpha < 30°$. The model parameters are summarized in Table 3.

The results of the calculated position-velocity diagram are plotted in Figure 14*b*. The empty pentagon symbols indicate the molecular gas, as distinct from the ionized gas (*dots*). There are several characteristics of the interacting gas shown in this velocity-declination diagram. In general, the central gravitational force produces a velocity gradient for the interacting molecular gas from an average radial velocity of $V_r = -165$ km s^{-1} at 2 pc north of the center to $V_r = -195$ km s^{-1} at 2 pc south of the center. This velocity gradient is consistent with the observed pattern (see Fig. 14*a*). The velocity dispersion along the line of sight is also calculated. The typical velocity dispersion generated by the interaction between the high-velocity gas and the central gravitational potential is 3–10 km s^{-1} in most regions. In the region 0.1–1 pc south of the center, the line-of-sight velocity dispersion produced by the gravitational interaction alone can be as large as 20 km s^{-1}. In addition, a high negative velocity wing which is located 0.5 pc south of the center and which extends up to -250 km s^{-1} can be produced by this model. The sensitivity of the existing OH observations may not be enough to detect the weak high-velocity wing. Alternatively, the radius of the central ionized cavity can be constrained by the distance between the dynamical center, presumably Sgr A*, and the location of the maximum velocity of the molecular wing. This high negative velocity wing at this particular location along with the velocity gradient are probably the unique signatures of the kinematics of the gas distorted by the central gravitational force.

TABLE 3

PARAMETERS FOR MODEL CALCULATIONS

Parameters	Value
Mass of the central scattering force	$4 \times 10^6\ M_\odot$
Incident velocity of a cloud	180 km s^{-1}
Incident angle	15°
Radius of central ionized region	0.6 pc
Extent of the cloud in front of the CND	10 pc

5.2. *Ionized Components and the Minicavity*

Furthermore, this model also predicts both a diffuse ionized component located northeast of the center in the velocity range from -180 km s^{-1} to $+100$ km s^{-1} and a compact component located near the incident region which is southwest of Sgr A* in the velocity range from -180 km s^{-1} to -400 km s^{-1}. The extreme value of the gas velocity depends on the exact value of *b*. The two ionized components are the by-products of this model. In a recent study of the ionized gas in the center of the Galaxy, a weak extended ionized component located

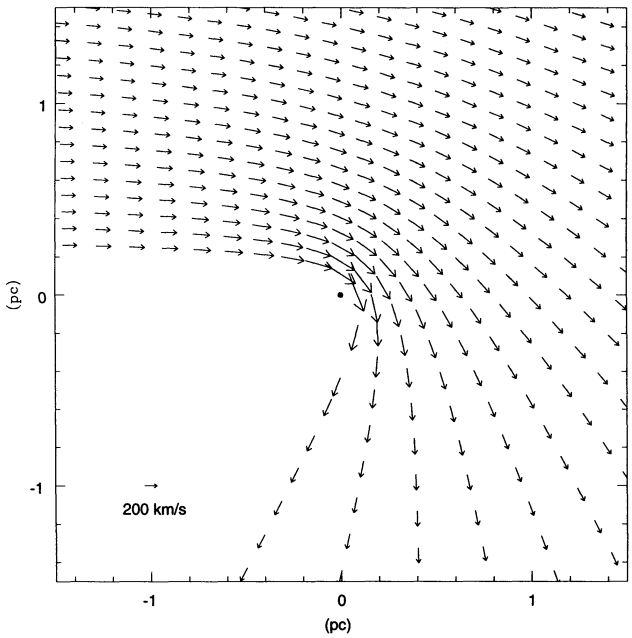

FIG. 11.—Two-dimensional velocity field of incident gas distorted by a central gravitational force in the central 3 pc of the Galctic center. The vectors indicate both the direction and magnitude of the gas velocity. The central black dot is the center of the gravitational field.

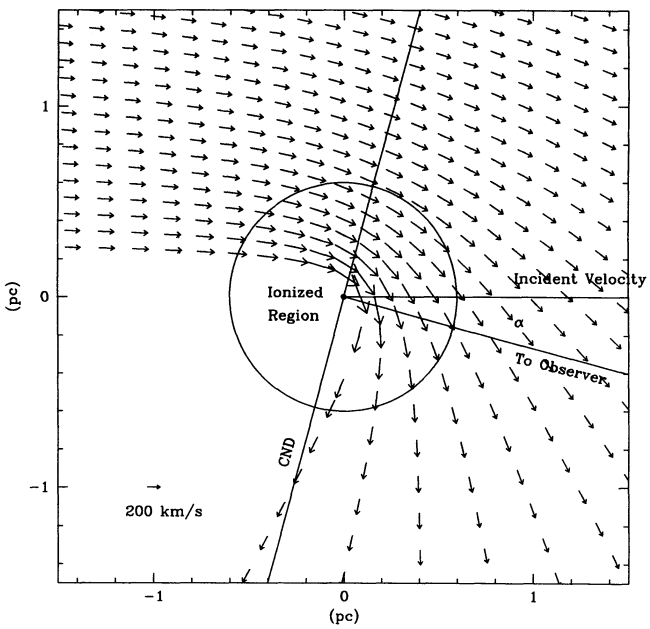

FIG. 13.—Structure of the incident velocities of the HNVG, CND, and line of sight used for the calculations of the position-velocity diagram (see Fig. 14). The solid line (CND) indicates the plane of the CND. The incident angle (α) between the incident velocity and the line of sight is marked. The circle indicates the ionizing zone with 0.6 pc in radius.

northeast of Sgr A* is detected in the radio recombination line (RRL) observations (Yusef-Zadeh et al. 1995). The velocity of this ionized component ranges from -195 to -130 km s^{-1}. The less negative velocities may not be detectable because of the contamination from the strong emission of the rotating ionized gas in the CND.

A compact ionized component located 5″ southwest of Sgr A* has also been detected at $V_r = -260$ km s^{-1} (e.g., Lacey et al. 1980; Serabyn et al. 1988; Roberts & Goss 1993). This feature has been shown by numerous high angular resolution observations (e.g., Lutz, Krabbe, & Genzel 1993; Herbst et al. 1993; Roberts et al. 1995) to be spatially coincident with the "minicavity." Note that the minicavity is not the OH cavity discussed in the previous sections and is a distinct hole in the distribution of the radio continuum emission with an angular size of 2″, centered at 3″.5 southwest of Sgr A* (Yusef-Zadeh, Morris, & Ekers 1989). Based on [Fe III] and Brγ observations, Lutz et al. suggest that the minicavity corresponds to an expanding bubble created by a fast (≥ 1000 km s^{-1}) wind from one or several sources 2″ within the minicavity; this wind also blows into the partially neutral gas streamers orbiting the dynamical center of the Galaxy. The detailed kinematics of the ionized gas surrounding the minicavity are shown in the H92α observations by Roberts et al. (1995) with high angular resolution (1″) and high velocity resolution (14 km s^{-1}). A large velocity gradient (600 km s^{-1} pc^{-1}) 4″ southeast of Sgr A* is observed. The most prominent feature at the high negative velocity of -280 km s^{-1} is located at the western rim of the minicavity. Both the high spatial and high velocity resolutions of the H92α observations make it possible to discriminate between different models for the ionized gas surrounding the minicavity. In particular, the detailed kinematics observed in H92α are difficult to explain with the wind model. The highly asymmetric kinematics with respect to Sgr A* are not consistent with *circular* rotation models.

The observations of OH and RRLs show an intimate relation between the ionized and the neutral molecular gas at the high negative velocity of -200 km s^{-1}. Both the morphology and the velocity suggest that the central RRL–emitting gas is a counterpart of the HNVG which impacts on the ionized "bar" in the center of the Galaxy (Lo & Claussen 1983). The impact of this high-velocity streamer results in a minicavity where the streamer gas is compressed. The density of the gas ($n_H > 10^5$

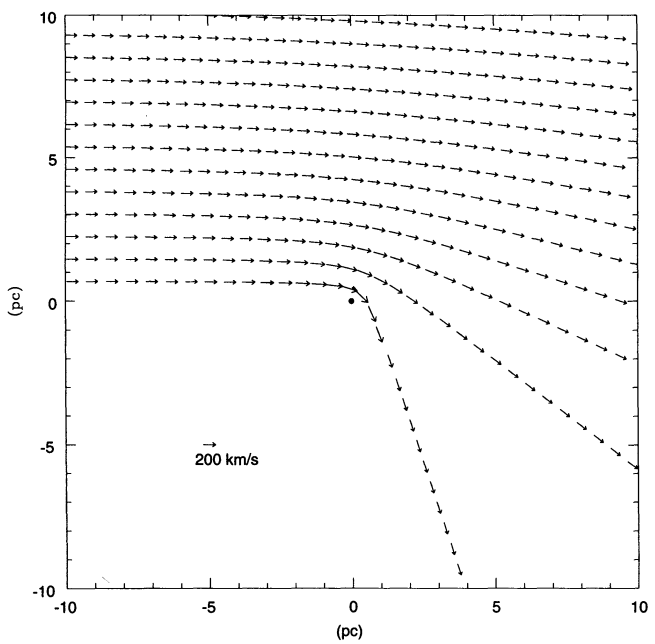

FIG. 12.—Two-dimensional velocity field of incident gas distorted by a central gravitational force in the central 10 pc of the Galaxy. The vectors indicate both the direction and magnitude of the gas velocity. The central black dot is the center of the gravitational field.

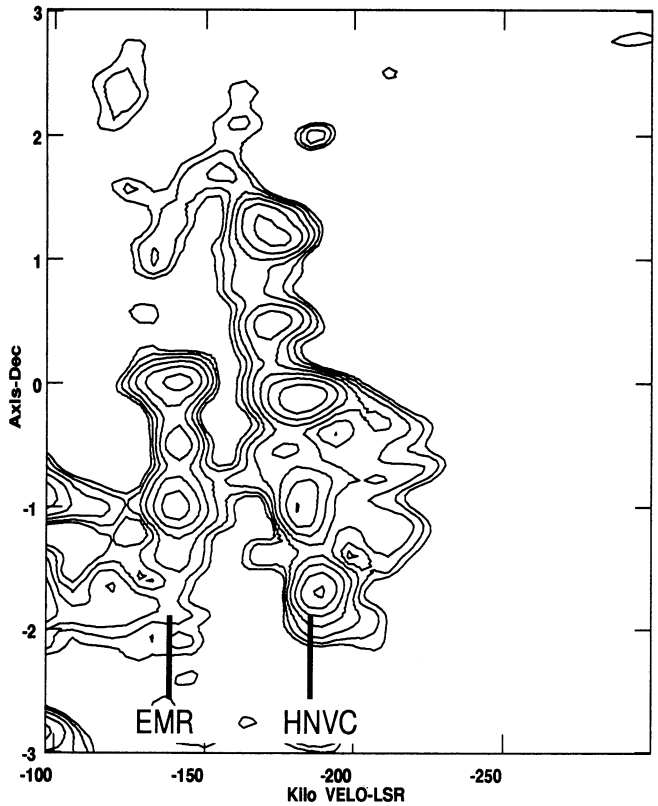

FIG. 14*a*

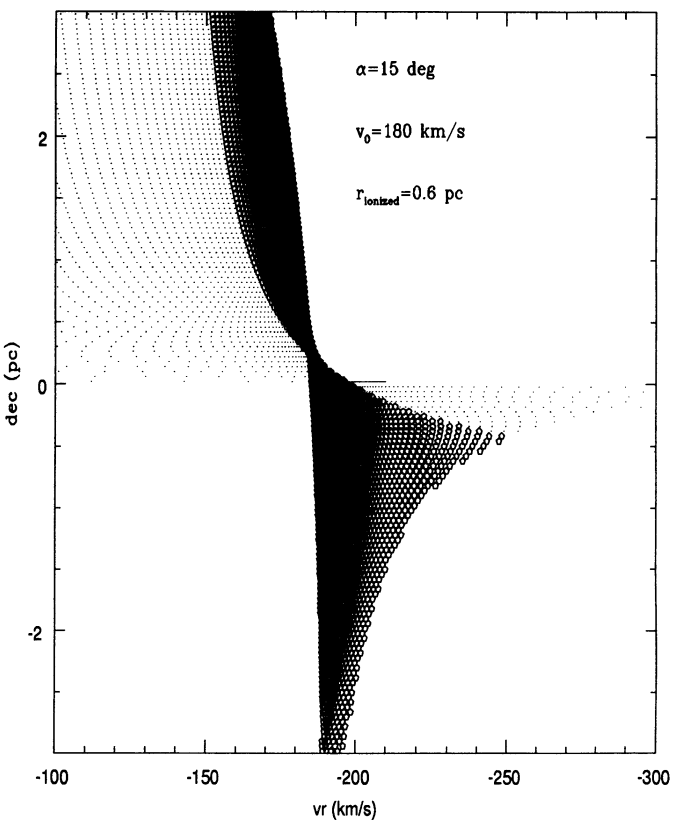

FIG. 14*b*

FIG. 14.—Velocity-declination diagrams. (*a*) Observation at the right ascension of Sgr A*. Both the HNVG and EMR are labeled. (*b*) Calculation from the model described in the text. The pentagon symbols represent the absorbing molecular gas, and the dots indicate the ionized gas.

cm^{-3}) determined from the surrounding ionized medium is large enough for a gas clump (>1″) within the minicavity to remain neutral; i.e., a column density of shielding materials of 10^{22} cm^{-2} could protect the molecular gas from destruction by the central UV radiation field (Marr et al. 1992) while the less dense, orbiting gas remains photoionized by the same UV radiation field.

We employ the same model as discussed for the OH data in the previous section to fit the central kinematics in the H92α data. The model parameters are summarized in Table 3. The impact parameter *b* is presumably small for the ionized gas. A range of *b* between 0.3 and 0.7 pc is assumed, which corresponds to the innermost five orbits plotted in Figure 13. Then we project these orbits on the plane of the sky with two free parameters, namely, the inclination and azimuth angles, in order to fit the observed radial velocity distribution. Figure 15 (Plate 1) shows the comparison of the radial velocity distribution observed with the H92α data (color-coded; Roberts et al. 1995) with the best-fitted projected orbits. The length of the vector indicates the magnitude of V_r, and the orientation indicates the direction of V_r. The hyperbolic orbit at motion can account for the detailed kinematics characterized by the large velocity gradient on the eastern edge of the minicavity (or southeast of Sgr A*) and the nearly constant velocity at −280 km s^{-1} along the southwest rim of the minicavity.

5.3. *Comments*

We have shown that the HNVG probably impacts on the center of the Galaxy. A dynamic model utilizing the central massive gravity has been discussed. This simple model succeeds in explaining the detailed kinematics of the HNVG observed over a range of angular scales from 1″ to 700″. There are, of course, some problems regarding the origin of the high-velocity cloud and how this cloud falls onto the Galactic center. Our model suggests that the cloud must be accelerated to a high velocity (180 km s^{-1}) prior to entering the central gravitational potential well. It is plausible that this HNVG cloud is a member of the high negative velocity cloud population observed over many degrees from the Galactic center (e.g., Wakker & van Woerden 1991; Mirabel & Morris 1984). Although the probability of a high velocity cloud directly impacting on the central parsec (or small impact parameter *b*) is thought to be very small, it is likely that such a cloud falls into the central degree of the Galaxy and is then tidally disrupted. The tidal instability may accelerate the debris of the disrupted cloud, i.e., reduce the values of the impact parameter. The overall elongated morphology (30 pc × 8 pc) in CO emission is consistent with this suggestion.

In addition, it is not clear whether the "flattened" east-west elongation in OH absorption is a proto–accretion disk. Further three-dimensional hydrodynamic modeling may be needed in order to understand the evolutionary process of a high-velocity cloud that interacts with the central gravitational potential with resulting filamentary structures.

6. CONCLUSION

We have detected the OH molecular absorption line at a velocity of −180 km s^{-1} in front of Sgr A* with an angular

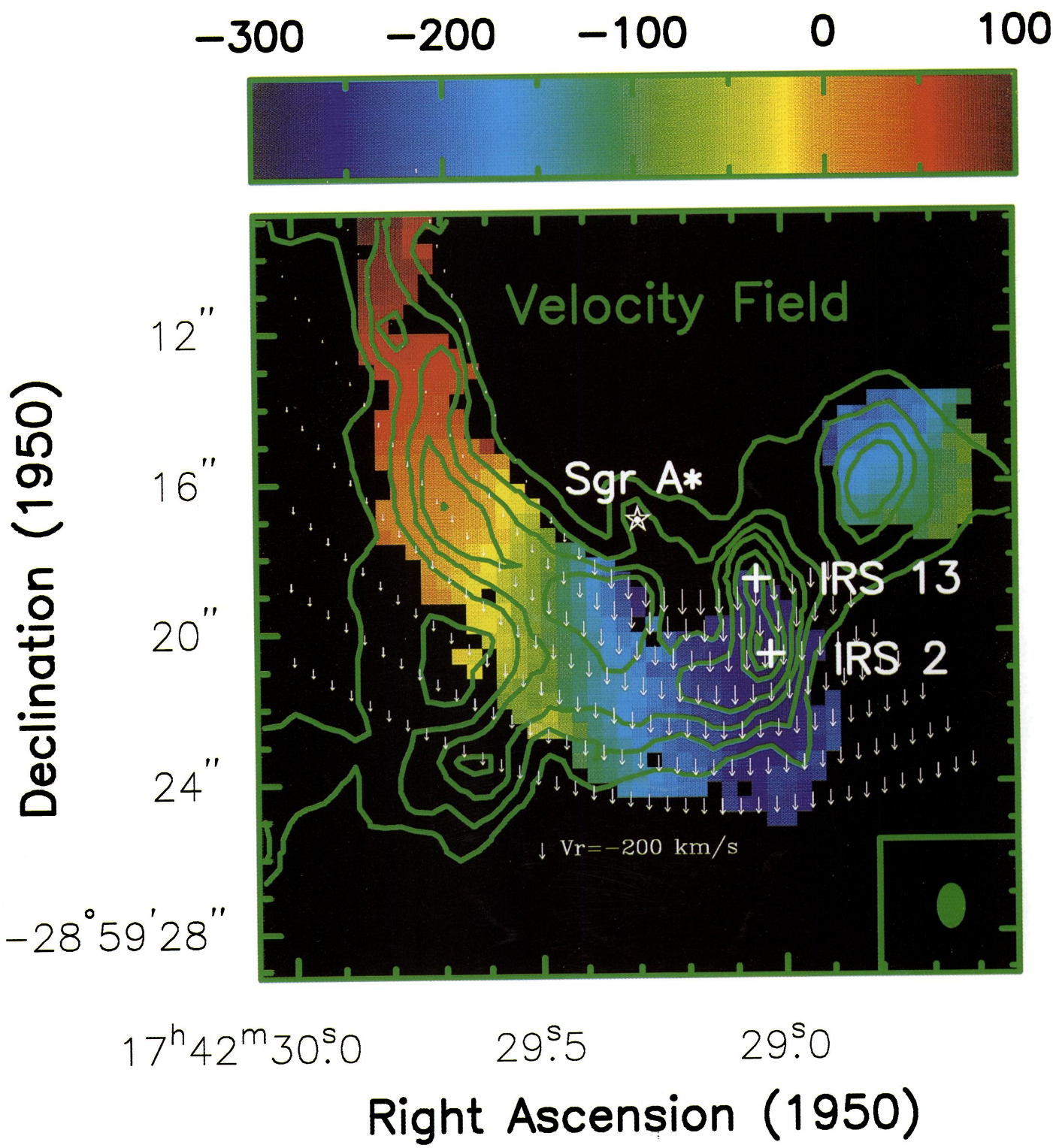

FIG. 15.—Color-coded velocity distribution image of the central 10″ of the Galaxy observed in the H92α (Roberts et al. 1995) with an angular resolution of 1″ and a velocity resolution of 14 km s^{-1} overlaid with radial velocity vectors calculated from the hyperbolic orbit model. This model, as discussed § 5.1, is based on the current OH data. In addition to the model parameters given in Table 3, a range of impact parameters b between 0.3 and 0.7 pc is assumed. We find that the inclination angle of 35° (0° for face on) and azimuth angle of −65° (counterclockwise from north) give the best fit to the H92α velocity image. The length of the vector gives the magnitude of the radial velocity. The direction of the vectors indicate direction only as positive (north) and negative (south) radial velocity.

ZHAO, GOSS, & HO (see 450, 135)

resolution of $\sim 1''$. Both the detailed structure and the kinematics of the absorbing gas have been imaged. The VLA OH observations provide evidence for locating the HNVG gas at the Galactic nucleus. The kinematic properties of the HNVG gas are unique and very different from those of the other gas components observed in the Galactic center region, such as the EMR and the rotating gas in the CND. Based on our analysis, the absorbing gas is a part of the high-velocity cloud seen in CO which is tidally disrupted and which flows toward the Galactic center.

A two-dimensional numerical model is produced based on the assumption that a high-velocity cloud interacts with the central gravitational potential. A velocity-declination distribution calculated from the dynamical model shows the detailed kinematic structures which agree with the observations. In addition, this model explains both the morphology and the kinematics observed in the H92α RRL within the central 10″ of the Galaxy.

We are grateful to Dan Gezari for providing the digital version of the 12.4 μm image and Doug Roberts for helpful discussion. The National Radio Astronomy Observatory is operated by Associated Universities, Inc., under cooperative agreement with the National Science Foundation.

REFERENCES

Allen, D. A., Hyland, A. R., & Hillier, D. J. 1990, MNRAS, 244, 706
Cornwell, T. J., Uson, J. M., & Haddad, N. 1992, A&A, 258, 583
Ekers, R. D., van Gorkom, J. H., Schwarz, U. J., & Goss, W. M. 1983, A&A, 122, 143
Gezari, D. 1992, in The Center, Bulge, and Disk of the Milky Way, ed. L. Blitz (Dordrecht: Kluwer), 23
Gezari, D., & Yusef-Zadeh, F. 1990, in AIP Conf. Ser., 14, Astrophysics with Infrared Arrays, ed. R. Elston (New York: AIP), 214
Güsten, R., & Downes, D. 1980, A&A, 87, 6
———. 1981, A&A, 99, 27
Güsten, R., Genzel, R., Wright, M. C. H., Jaffe, D. T., Stutzki, J., & Harris, A. I. 1987, ApJ, 318, 124
Herbst, E., & Leung, C. M. 1989, ApJS, 69, 271
Herbst, T. M., Beckwith, S. V. W., Forrest, W. J., & Pipher, J. L. 1993, AJ, 105, 956
Ho. P. T. P., Ho, L. C., Szczepanski, J. C., Jackson, J. M., Armstrong, J. T., & Barrett, A. H. 1991, Nature, 350, 309
Jackson, J. M., Geis, N., Genzel, R., Harris, A. I., Madden, S., Poglitsch, A., Stacey, G. J., & Townes, C. H. 1993, ApJ, 402, 173
Krabbe, R., Genzel, R., Drapatz, S., & Rotaciuc, V. 1991, ApJ, 382, L19
Lacy, J. H., Townes, C. H., Geballe, T. R., & Hollenbach, D. J. 1980, ApJ, 241, 132
Liszt, H. S., & Burton, W. B. 1993, ApJ, 407, L25
Liszt, H. S., Burton, W. B., Sanders, R. H., & Scoville, N. Z. 1977, ApJ, 213, 38
Lo, K. Y., & Claussen, M. J. 1983, Nature, 306, 647
Lutz, D., Krabbe, A., & Genzel, R. 1993, ApJ, 418, 244
Marr, J. M., Rudolf, A. L., Pauls, T. A., Wright, M. C., & Backer, D. C. 1992, ApJ, 400 L29
Marshall, J., & Lasenby, A. 1994, MNRAS, 269, 619
———. 1995, in preparation
Mirabel, I. F., & Morris, R. 1984, ApJ, 279, 86
Pauls, T., Johnston, K. J., Wilson, T. L., Marr, J. M., & Rudolph, A. 1993, ApJ, 403, L13
Pedlar, A., Anantharamaiah, K. R., Ekers, R. D., Goss, M. W., van Gorkom, J. H., Schwarz, U. J., & Zhao, J. 1989, ApJ, 342, 769
Roberts, D. A., & Goss, W. M. 1993, ApJS, 86, 133
Roberts, D. A., Yusef-Zadeh, F., & Goss, W. M. 1995, ApJ, submitted
Sanders, R. H., Wrixon, G. T., & Mebold, U. 1977, A&A, 61, 329
Schwarz, U. J., Bregman, J. D., & van Gorkom, J. H. 1989, A&A, 215, 33
Scoville, N. Z. 1972, ApJ, 175, L127
Serabyn, E., Lacy, J. H., Townes, C. H., & Bharat, R. 1988, ApJ, 326, 171
Wakker, B. P., & van Woerden, H. 1991, A&A, 250, 509
Yusef-Zadeh, F., Lasenby, A., & Marshall, J. 1993, ApJ, 410, L27
Yusef-Zadeh, F., Morris, M., & Ekers, R. D. 1989, in The Center of the Galaxy, ed. M. Morris (Dordrecht: Kluwer), 443
Yusef-Zadeh, F., Zhao, J.-H., & Goss, W. M. 1995, ApJ, 442, 646
Zhao, J.-H., et al. 1992, Science, 255, 1538